Quantification of water yield concerning land use and climate scenarios in the Tajan watershed, North of Iran

F. Ahmadi-Mirghaed[1] · M. Rahmani[1] · S. Molla-Aghajanzadeh[1]

Abstract

Water yield (WY) is a key provisioning ecosystem services that is sensitive to climate and land use changes. This study aimed to evaluate the impacts of climate and land use changes on WY in the Tajan watershed, northern Iran, from 2022 to 2052. Additionally, it investigated the relationship of WY to slope, elevation, and normalized difference vegetation index (NDVI) specifically in 2022. Land use change was simulated in the TerrSet v19 software using the Land Change Modeler, while climate change was projected based on the CMCC-CM model under RCP45 and RCP85 scenarios using the LARS-WG 6 software. Six scenarios were designed according to climate and land use to evaluate the WY in the InVEST 3.13 software. Statistical analysis was performed using the Getis-Ord (G*) statistic, bivariate local Moran's I (BLMI), and geographically weighted regression (GWR). The results revealed that WY had hotspots in the northern parts and cold spots in the central parts. The total WY volume ranged from 8.7 to 25.1 $\mathrm{Mm^3\ y^{-1}}$ based on all scenarios. It was clarified that land use change increased WY by 2–7%, while climate change decreased it by 47% and 65% under RCP45 and RCP85, respectively. The lowest WY was observed in the forest, while and the highest was in built-up areas. As indicated by the BLMI, the WY had a moderate spatial autocorrelation to elevation and slope, having Moran's I of -0.53 and -0.62, respectively. In contrast, its spatial autocorrelation with NDVI was weak with Moran's I of -0.01. The GWR analysis revealed a significant spatial correlation of WY to elevation, slope, and NDVI, having R^2 values of 0.94, 0.90, and 0.96, respectively. This study showed that climate change has a greater impact on the WY than land use change. Furthermore, WY distribution is influenced by topography and vegetation. Therefore, it is necessary to implement regional management plans through water conservation policies and dealing with climate and land use changes to conserve the water resources of the Tajan watershed in the future.

Keywords Water yield · Climate change · Land use change · Spatial analysis · InVEST

Introduction

Human societies rely heavily on natural ecosystems, which are self-organizing systems that provide a range of services to humans, including water, food, wood, fiber, agricultural products, and raw materials. Additionally, ecosystems maintain a balance among the different components of the environment, preserving biodiversity and purifying the environment (Costanza et al. 1997; Daily 1997; Millennium

Ecosystem Assessment 2005). Each ecosystem has a unique structure and function that is significantly impacted by human activity and climate change. In recent decades, global climate change has posed a major threat to the preservation and sustainability of ecosystem services. According to the Millennium Ecosystem Assessment, approximately 60% of identified ecosystem services are degraded. Without proper management and planning, this degradation is expected to increase over the next 50 years (Millennium Ecosystem Assessment 2005; Wang et al. 2016).

Water yield (WY) is an ecosystem service that is affected by climate and land use changes (Guo et al. 2023; Hu and Gao 2020; Pei et al. 2022; Tijjani et al. 2022; Wang et al. 2016). It refers to the availability of water resources in a watershed, which is influenced by changes in precipitation and evapotranspiration. WY is estimated based on the difference between precipitation and evapotranspiration. This

✉ M. Rahmani
m.rahmani@umz.ac.ir

[1] Department of Environmental Sciences, Faculty of Marine and Environmental Sciences, University of Mazandaran, Babolsar, Iran

estimation is influenced by various factors, including climate change, agricultural and human activities, urban development, population growth, and global warming, which can cause significant changes in precipitation and evapotranspiration, ultimately leading to a reduction in WY. Therefore, it is essential to assess and measure the effects of climate change and human activities on WY to preserve and allocate water resources rationally across various regions (Guo et al. 2023; Tijjani et al. 2022; Xiao et al. 2020; Yifru et al. 2021).

Previous studies have investigated the impacts of climate and land use changes on WY. Guo et al. (2023) used the Integrated Valuation of Ecosystem Services and Tradeoffs (InVEST) tool to examine the effects of climate and land use changes on WY in 17 sub-basins across China. They confirmed that these factors had serious impacts on WY according to the climatic, geographical, and socio-economic characteristics of the sub-basins. By utilizing the InVEST model, Mirghaed and Souri (2023) simulated WY in the Shoor River basin, southwestern Iran, and evaluated its relationship with land use changes, soil characteristics, and topographic features. Their study found that the topographic features had a higher contribution on WY than soil properties. Amiri et al. (2023) assessed the impacts of land use and climate change on the hydrological regime of the Tajan River in northern Iran using the soil and water assessment tools (SWAT). They reported that climate and land use changes will lead to water stress in their study region in the coming decades. Huang et al. (2023) conducted a study to investigate the changes in ecosystem services of WY and carbon sequestration in China's Loess Plateau by combining InVEST and Carnegie-Ames-Stanford Approach (CASA) models. They concluded that climate change and human activities have mainly influenced the increase of WY in the region since 2001. Pei et al. (2022) analyzed annual changes in WY and their relationship with revegetation in northern China, encompassing past, present, and future effects. Their research indicated that changes in climate and land use were responsible for 88% and 12% of the changes in WY, respectively, from 2000 to 2019. Tijjani et al. (2022) used the General Circulation Model (GCM)-based SWAT model for two representative concentration pathways (RCP) namely RCP45 and RCP85 to assess the effects of short-term climate change on irrigation demand, green water scarcity, and crop yield in an agricultural watershed in southern New Jersey, USA. Their study demonstrated that increases in precipitation and temperature result in higher surface runoff, groundwater recharge, lateral flow, and total stream flow. Rafiei-Sardooi et al. (2022) simulated the effects of land use and climate change on WY, water supply, and water consumption in the Halil River basin in Iran using the InVEST software. In their study, the HadGEM2-ES model under RCP26, RCP45, and RCP85 was used to assess climate change, and the land change modeler (LCM) in TerrSet v19

was applied to map land use change. Daneshi et al. (2021) investigated the yield, supply, and consumption of water in a catchment in northern Iran using the WY model of the InVEST tool. They conducted a combined modeling of the effects of climate and land use scenarios on water security to estimate the water stress and economic costs associated with reducing WY in the future. Benra et al. (2021) assessed WY using the InVEST in 224 watersheds in southern Chile. They conducted this study for three years, 1998, 2007, and 2013 to investigate the effects of land use and climate change. Hu and Gao (2020) modeled WY over Shaanxi-Gansu Loess Plateau in China under climate and land use scenarios using the InVEST tool. Their study showed that the impact of climate change on the WY is much higher than that of land use change.

The impacts of land use and climate changes on the WY have been studied in various regions worldwide. Nevertheless, there have been limited investigations into their interactive effect on the WY in Iran. In previous studies, other critical factors such as topography and vegetation, which could impact the WY, have not been adequately evaluated. The Tajan watershed is a crucial component of the Hyrcanian forest ecosystem in northern Iran, serving as a vital habitat and ecological resource, as well as playing a significant role in providing regional water resources. In recent decades, environmental tensions and crises have arisen due to climate and land use changes, which have affected water resources and productivity in this region. Consequently, habitat conditions for humans and other creatures have been impacted. Therefore, this study investigated how land use and climate changes impact WY in the Tajan watershed, located in the north of Iran. Additionally, it sought to determine the relationship of WY to topography (slope and elevation) and vegetation (NDVI: Normalized Difference Vegetation Index). The study objectives were: (i) the simulation of climate and land use changes in the Tajan watershed over a 30-year period (2022 to 2052), (ii) the modeling of WY in the study area using climate and land use scenarios through the InVEST 3.13 software, and (iii) the assessment of the relationships of WY to elevation, slope, and NDVI at the sub-watershed level of the region in 2022.

Materials and methods

Study area

The Tajan River watershed, covering an area of about 4720 km², is situated between 52° 18′ 17″ E to 54° 9′ 8″ E and 35° 55′ 57″ N to 36° 49′ 26″ N in Mazandaran province, northern Iran (Fig. 1). It boasted an average elevation and annual temperature of 1179 m and 25 °C,
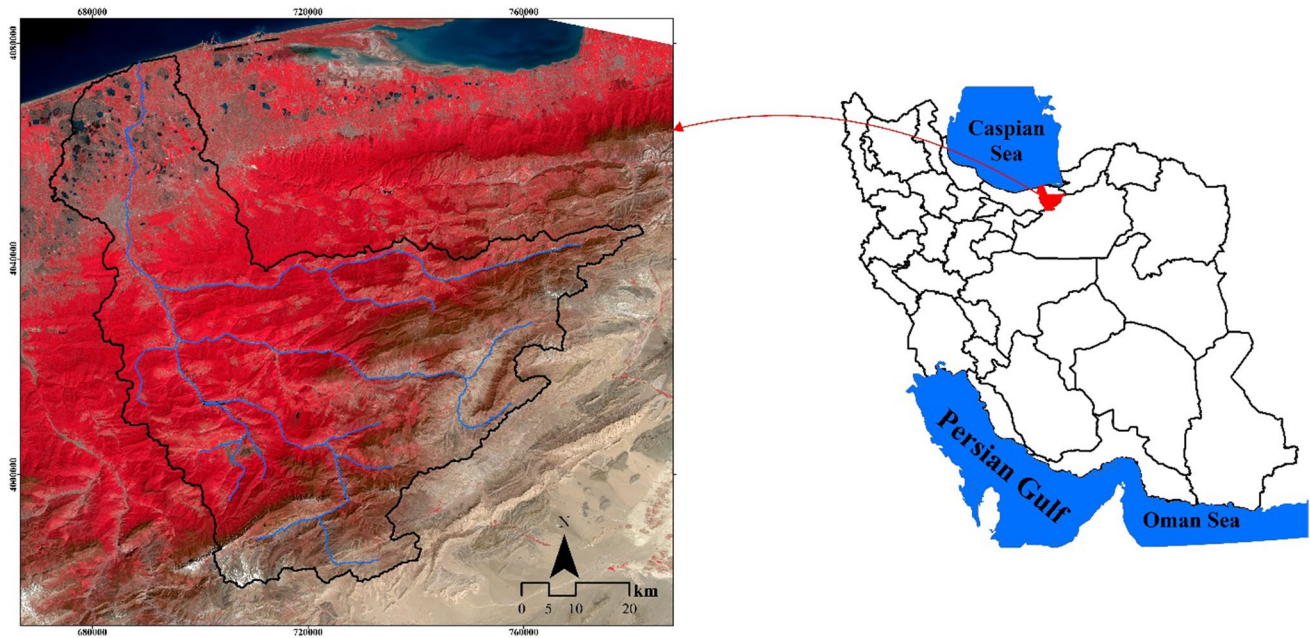
Fig. 1 Geographical location of the study area

respectively. The region is predominantly composed of mountains, plains, and coastal plains, which account for around 85% of its terrain. The remaining 15% is occupied by foothills, hills, and river terraces. Agriculture and construction dominate the plains in the north, while forests and rangelands are found in the mountainous regions of the south and central watershed. The tributaries of the Tajan River, originating from the southern region, flow through the lowlands and highlands of the watershed, ultimately leading to the Caspian Sea. Most of the area is covered by Hyrcanian forests, demonstrating the ecological significance of its habitats for conserving biodiversity.

Data collection

The dataset utilized in this study is presented in Table 1. The digital elevation model (DEM) was extracted from the shuttle radar topography mission (SRTM) images through the google earth engine (GEE). The GEE was also used to download Landsat 5, 7 and 8 images to create land use maps for 1992, 2012 and 2022. The meteorological statistics from 14 stations in and around the region spanning 30 years (1992–2022) have been used to gather data on precipitation, temperature, and radiation. The plant available water content was estimated based on soil's clay, sand, silt, and organic matter percentages,

obtained from global soil grid data downloaded from the GEE.

Land use change simulation

Land use maps for the study area in 1992, 2012, and 2022 were created by analyzing surface reflectance images from Landsat 5, 7 and 8, respectively, downloaded from the GEE platform and classified using a support vector machine (SVM) algorithm in the ENVI 5.3 software. The classification accuracy was evaluated through visual interpretation and a confusion matrix. The matrix was based on ground reference points taken from Google Earth images and used to calculate statistics including user's accuracy (UA), producer's accuracy (PA), commission error (CE), omission error (OE), overall accuracy (OA), and kappa coefficient. The statistics were computed using the following equations (Eastman 2012):

$$UA = \frac{1}{n}\left(\sum_{i=1}^{n}\frac{P_{ir}}{P_{tr}}\right) \times 100 \qquad (1)$$

$$PA = \frac{1}{m}\left(\sum_{j=1}^{m}\frac{P_{jc}}{P_{tc}}\right) \times 100 \qquad (2)$$

$$CE = 1 - UA \qquad (3)$$

Table 1 Dataset used in this study

Data	Type/ Resolution	Description/Explanation	Source/References
Elevation (m)	Raster, 30 m	Extracted from the digital elevation model of the study area prepared from the SRTM images	https://code.earthengine.google.com
Slope (%)	Raster, 30 m	Prepared based on digital elevation model and using slope module in ArcGIS 10.7 software	
NDVI	Raster, 30 m	Created using surface reflectance images of the red and infrared bands of Landsat 5 and 8 (related to 1992 and 2022, respectively) in the Google Earth Engine system	https://code.earthengine.google.com
Land use	Raster, 30 m	Prepared using the SVM method in ENVI 5.3 software based on Landsat images for 1992 and 2022	https://code.earthengine.google.com
Precipitation (mm)	Point	Extracted from the statistics of 14 meteorological stations in and around the study area	https://www.irimo.ir
Temperature (°C)	Point	Extracted from the statistics of 14 meteorological stations in and around the study area	https://www.irimo.ir
Radiation (MJ m^{-2} d^{-1})	Point	Extracted from the statistics of 14 meteorological stations in and around the study area	https://www.irimo.ir
Evapotranspiration (mm)	Point	Calculated based on temperature, precipitation and radiance data according to Eq. 8	
Root restricting layer depth (mm)	Raster, 30 m	Extracted from global soil grid data	https://www.isric.org
Available water content	Raster, 30 m	Extracted from global soil grid data	https://www.isric.org
Plant available water content	Raster, 30 m	Calculated based on the percentage data of clay, silt, sand and soil organic matter extracted from global soil grid data according to Eq. 9	https://www.isric.org
Sub-watersheds	Vector	Produced based on the digital elevation model of the study area and using the ArcHydro extension in ArcGIS 10.7 software	
Kc	Decimal	Extracted from scientific sources	Mirghaed and Souri (2022)

$$OE = 1 - PA \tag{4}$$

$$OA = \frac{P_c}{P_t} \times 100 \tag{5}$$

$$Kappa = \frac{P_t \times \sum_{i=1}^{k} P_c - \sum_{i=1}^{k} P_{ir} \times P_{jc}}{P_t^2 - \sum_{i=1}^{k} P_{ir} \times P_{jc}} \tag{6}$$

where P_{ir} and P_{jc} represent the number pixels correctly classified in row i and column j of the error matrix, respectively. P_{tr} and P_{tc} show the total number of pixels in row i and column j, respectively. P_c is the number of correctly classified pixels, while P_t shows the total number of evaluating pixels. n and m are the number of rows and columns of the error matrix. It should be noted that the kappa coefficient greater than 0.8 indicates acceptable classification accuracy (Shivakumar and Rajashekararadhya 2018).

The land change modeler (LCM) in the TerrSet v19 software was utilized to project land use changes for 2052. The LCM model integrates the Markov chain model, multi-layer perceptron neural network, logistic regression, and multi-objective land allocation, thereby rendering it highly efficient in simulating land use changes. The LCM modeling follows four crucial steps, namely assessment of land use changes, modeling of transition force, modeling of land use change, and accuracy assessment. In the transition force modeling, the LCM model utilizes auxiliary variables to evaluate the potential of each pixel of an image to change from one land use type to another. Auxiliary variables are drivers that influence land use change. The correlation between variables and land use is measured using Cramer's V, which ranges from 0 to 1. Variables with a Cramer's V greater than 0.15 are considered useful for predicting land use changes (Eastman 2012).

In this study, the land use maps of 1992 and 2022 served as inputs of the LCM model to project land use map of 2052. The study utilized several auxiliary variables, including elevation, slope, aspect, distance from roads, distance from residential centers, distance from agricultural lands, distance from rangelands, and distance from waterbodies. These variables were selected based on the environmental conditions of the region and Cramer's V higher than 0.15. The model was validated by comparing the 'reference'

map (the land use map of 2022 produced using the SVM method) with the 'comparison' map (the predicted land use map of 2022). The projected map of 2022 was created using the LCM model and the land use maps of 1992 and 2012. To measure the validity and accuracy of the model, the kappa values (Kno, Klocation, KlocationStrata, and Kstandard), and the statistics of DisagreementGridCell, DisagreementQuantity, AgreementQuantity, AgreementChance, AgreementGridCell, Hits, False Alarms, and Misses were calculated using the Validation module in TerrSet v19 software (Eastman 2012; Leta et al. 2021). For more information about the statistics, refer to Pontius and Suedmeyer (2004), Eastman (2012) and Leta et al. (2021).

Climate change projection

Various tools and models have been developed to project climate change. LARS-WG 6 has been frequently employed to project future climate changes through various global circulation models (GCMs). It is a user-friendly open-source tool that can simulate future climate scenarios based on different greenhouse gas emission scenarios (Semenov et al. 2002). By applying the LARS-WG 6 software, climate changes in the study area were projected for 2052 based on the CMCC-CM model under two different representative concentration pathways (RCP) scenarios, namely RCP45 and RCP85. The CMCC-CM model outperforms other GCMs for simulating climate parameters, specifically temperature and precipitation, over Iran (Abbasian et al. 2019). The model was supplied with data inputs comprising of the daily minimum temperature, daily maximum temperature, daily precipitation, and daily radiation collected from 14 different meteorological stations situated in and around the region.

Water yield modeling

InVEST models WY using average annual rainfall (P_x), actual evapotranspiration (AET_x), reference evapotranspiration (ET_0), plant available water content ($PAWC$), edaphic-climatic characteristics, root-limiting soil depth and land use based on the water balance hypothesis according to Eq. 7 (Guo et al. 2023; Sharp et al. 2020).

$$WY = \left(1 - \left(\frac{AET_x}{P_x}\right)\right) * P_x \qquad (7)$$

where WY, P_x, and AET_x are based on mm/pixel. The ratio of AET_x/P_x for each land use is determined by applying the Budyko curve expression (Fu 1981; Zhang et al. 2004).

$$\frac{AET_x}{P_x} = 1 + \frac{PET_x}{P_x} - \left[1 + \left(\frac{PET_x}{P_x}\right)^{\omega}\right]^{1/\omega} \qquad (8)$$

where PET_x represents potential evapotranspiration and ω is an empirical parameter that represent natural edaphic-climatic characteristics (Donohue et al. 2012; Hargreaves and Samani 1982).

$$PET_x = k_c(l_x) \times ET_0 \qquad (9)$$

where ET_0 is the reference evapotranspiration and K_c (ℓx) is the plant evapotranspiration coefficient on pixel x. K_c regulates the ET_0 values based on the crop type or vegetation cover. ET_0 can be calculated using the following equation (Droogers and Allen 2002):

$$ET_0 = 0.0013 \times 0.408 \times RAD \times (T_m + 17) \times (T_d - 0.0123P)^{0.76} \qquad (10)$$

where RAD refers to the extraterrestrial radiation ($MJ\ m^{-2}\ d^{-1}$). T_m shows the daily average maximum and minimum temperatures (°C). T_d is the difference between the daily average minimum and maximum temperatures (°C). P specifies the monthly precipitation (mm).

PAWC, or plant-available water capacity, denotes the available water supply to plants, determined as the contrast between the field capacity and the permanent wilting point. The calculation for this is as follows (Sharp et al. 2020):

$$PAWC = 54.509 - 0.132 \times SA\% - 0.003 \times (SA\%)^2 - 0.055 \times SI\% - 0.006 \times (SI\%)^2$$
$$- 0.738 \times CL\% + 0.007 \times (CL\%)^2 - 2.688 \times OM\% + 0.501 \times (OM\%)^2 \qquad (11)$$

where $CL\%$, $SA\%$, $SI\%$, and $OM\%$ demonstrate the percentage of clay, sand, silt, and organic matter, respectively. The model was calibrated using the Z parameter, an empirical index that expresses the local rainfall pattern and hydrological characteristics estimated using Eq. 12.

$$Z = \frac{(\omega - 1.25)P_x}{AWC} \qquad (12)$$

Available water content (AWC) is the volume (mm) of the water that can be held by plants, determined by soil texture and effective rooting depth. It was calculated in this study using global soil grid data (Sharp et al. 2020). For more information about WY-InVEST model, refer to Sharp et al. (2020).

Table 2 Description of Land use and climate scenarios

Scenario	Land use	Climate	Explanation
LC22	2022	2022	Implemented based on the land use and climate conditions of 2022
LC52	2052	2022	Implemented based on the land use of 2052 and the climate conditions of 2022
CC45	2022	2052	Implemented based on the land use of 2022 and the climate conditions of 2052 projected according to RCP45
CC85	2022	2052	Implemented based on land use of 2022 and climate conditions of 2052 projected according to RCP85
LCC45	2052	2052	Implemented based on the land use of 2052 and the climate conditions of 2052 projected according to RCP45
LCC85	2052	2052	Implemented based on land use of 2052 and climate conditions of 2052 projected according to RCP85

Water yield scenarios

Six scenarios were designed based on land use and climate factors (precipitation and evapotranspiration) to project WY in the watershed for 2022 and 2052. As described in Table 2, each scenario considered the impacts of land use change, or climate change, or their combined effects on WY. The scenarios were implemented in the InVEST 3.13 software by altering the inputs of the WY model, including annual precipitation, evapotranspiration, and land use.

Statistical analysis

The study employed statistical analyses of the Getis-Ord (G*) statistic, bivariate local Moran's I (BLMI), and geographically weighted regression (GWR) to investigate the relationships under examination. The G* statistic is used to assess the spatial autocorrelation of a variable and identify its hot and cold spots in space, with values greater than the average denoting a high-high cluster or hot spot, and those smaller than the average indicating a low-low cluster or cold spot. BLME can be used to evaluate the spatial autocorrelation of two variables and is more effective than the G* statistic. The x-axis of the Moran scatter plot shows one variable, while the y-axis displays the spatial lag of another variable. The closer Moran's I is to $+1$ or -1, the stronger the spatial autocorrelation, and if it approaches zero, it indicates weaker spatial autocorrelation (Anselin 1995; Getis and Ord 1992;

Ord and Getis 1995). The GWR is an extended form of ordinary least square (OLS) regression that evaluates the spatial correlation between two variables by considering their local spatial relationships. It examines heterogeneous spatial relationships between dependent and independent variables at every geographic location in an unstable space. This method enables the assessment of local correlation between geographic parameters (Brunsdon et al. 1998; ESRI 2016).

By applying the GeoDa 1.18 software, the G* statistic was used to investigate the hot and cold spots of WY at the sub-watershed level. Spatial autocorrelation of WY to elevation, slope, and NDVI was assessed through the BLMI statistic. Additionally, the spatial correlation of WY with elevation, slope, and NDVI was also evaluated using the GWR in ArcGIS 10.7. These statistical analysis were conducted with data from the region in 2022.

Results and discussion

Land use and climate changes

Figure 2 indicates the land use maps of 1992 and 2022, as well as the projected map of 2052 generated using the LCM model. Notably, the land use classification accuracy of 1992 yielded a kappa coefficient, overall accuracy, producer's accuracy, user's accuracy, omission error, and commission error of 0.90, 93%, 91%, 95%, 9% and 5%, respectively. For
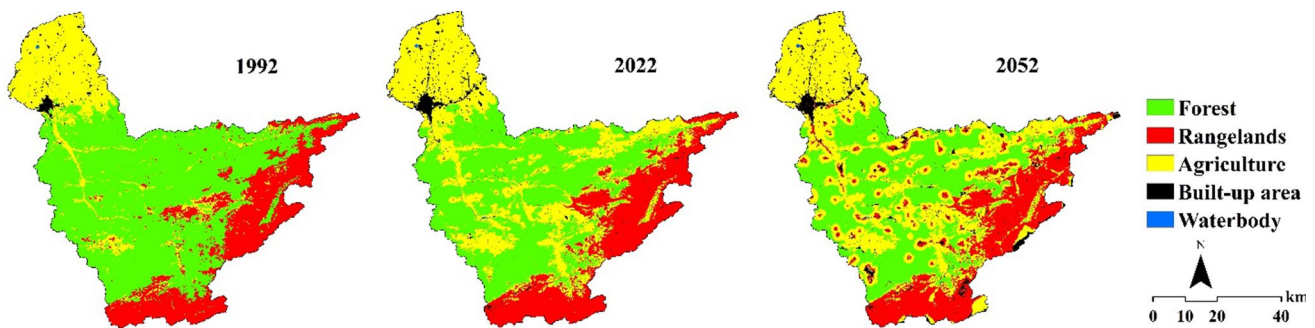

Fig. 2 Land use maps of the study area for 1992, 2022, and 2052

Table 3 The area allocated to each land use in 1992, 2022 and 2052 and their changes

| Land use	1992		2022		2052		1992–2022		2022–2052	
	ha	%	ha	%	ha	%	ha	%	ha	%
Forest	274,358	58	195,918	42	139,578	30	− 78,440	− 17	− 56,340	− 12
Rangelands	101,012	21	100,599	21	102,717	22	− 413	− 0.1	+ 2117	+ 0.4
Agriculture	92,447	20	165,110	35	211,338	45	+ 72,663	+ 15	+ 46,229	+ 10
Built-up area	3753	1	9849	2	17,840	4	+ 6097	+ 1	+ 7991	+ 2
Waterbody	393	0.08	487	0.1	490	0.1	+ 94	+ 0.02	+ 3	+ 0.001
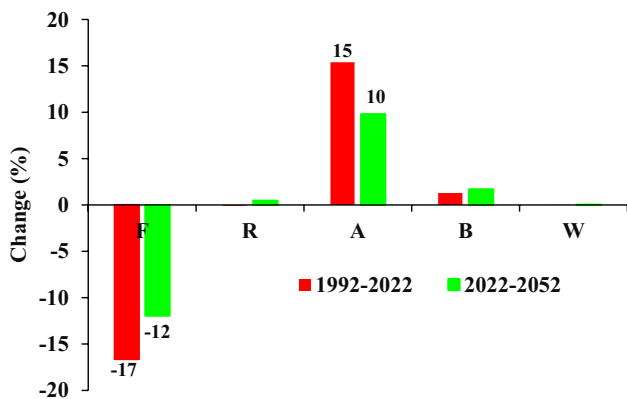
**Fig. 3** Land use change in the study area during the periods of 1992–2022 and 2022–2055

the 2022 land use classification, these metrics were estimated at 0.91, 94%, 93%, 92%, 7% and 8%, respectively. These results demonstrated the classifications' acceptable validation and accuracy. Ambarwulan et al. (2023) calculated the kappa coefficient and overall accuracy for modeling land use changes in the Cisadane watershed in Indonesia to be over 83%. Sisay et al. (2023) estimated the kappa coefficient and overall accuracy in land use classification in the Goang watershed, Ethiopia, for different years to be higher than 84% and 86%, respectively. The model validation and accuracy were proven by the estimated kappa values (Kno = 0.97, Klocation = 0.98, KlocationStrata = 0.98, and Kstandard = 0.96) being above 0.8 (Viera and Garrett 2005).

Additionally, the statistics of DisagreementGridCell, DisagreementQuantity, AgreementQuantity, AgreementChance, AgreementGridCell, Hits, False Alarms, and Misses were recorded as 0.01, 0.01, 0.20, 0.14, 0.64, 16.1%, 1.6%, and 0.9%, respectively. These findings proved the acceptability of the model's predictions (Eastman 2012; Leta et al. 2021). The area allocated to each land use is specified in Table 3. From 1992 to 2022, the forest, rangelands, agriculture, built-up areas, and waterbodies decreased by − 78,440, − 413, + 72,663, + 6097 and + 94 ha, respectively. Predictions showed that from 2022 to 2052, the mentioned land uses will further decrease by − 56,640, + 2117, + 46,229, + 7994, and + 3 ha, respectively.

The study revealed that the region experienced significant land use changes from 1992 to 2022. Approximately 22% (102,960 ha) of the region was affected by such changes. Forests experienced the highest decrease (-17%), while agricultural land increased the most (+ 15%) (Fig. 3). It is predicted that 17% (equal to 81,113 ha) of the watershed will undergo land use conversion from 2022 to 2052. Forests will experience the highest decline (− 12%), while agriculture will have the highest increase (+ 10%). In addition, Fig. 4 shows the changes in precipitation and evapotranspiration in the sub-watersheds of the region from 1992 to 2052. Precipitation and evapotranspiration exhibited a rising trend from 1992 to 2022, with downward and upward trends forecasted for them from 2022 to 2052, respectively. The evaluation of uncertainty in predicting climate parameters was based on observational and historical data. The correlation coefficient and the normalized root mean square error
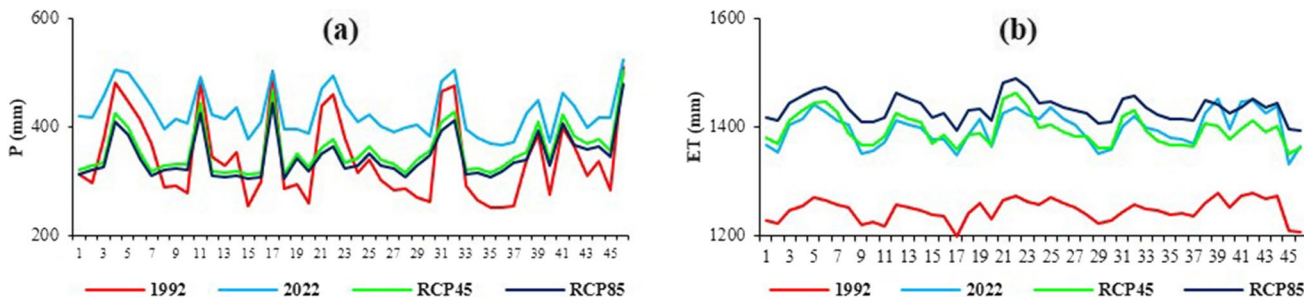
Fig. 4 Changes in **a** precipitation (P) and **b** evapotranspiration (ET) of the study area in 1992, 2022, and 2052. P and ET related to 2052 are projected based on RCP45 and RCP85
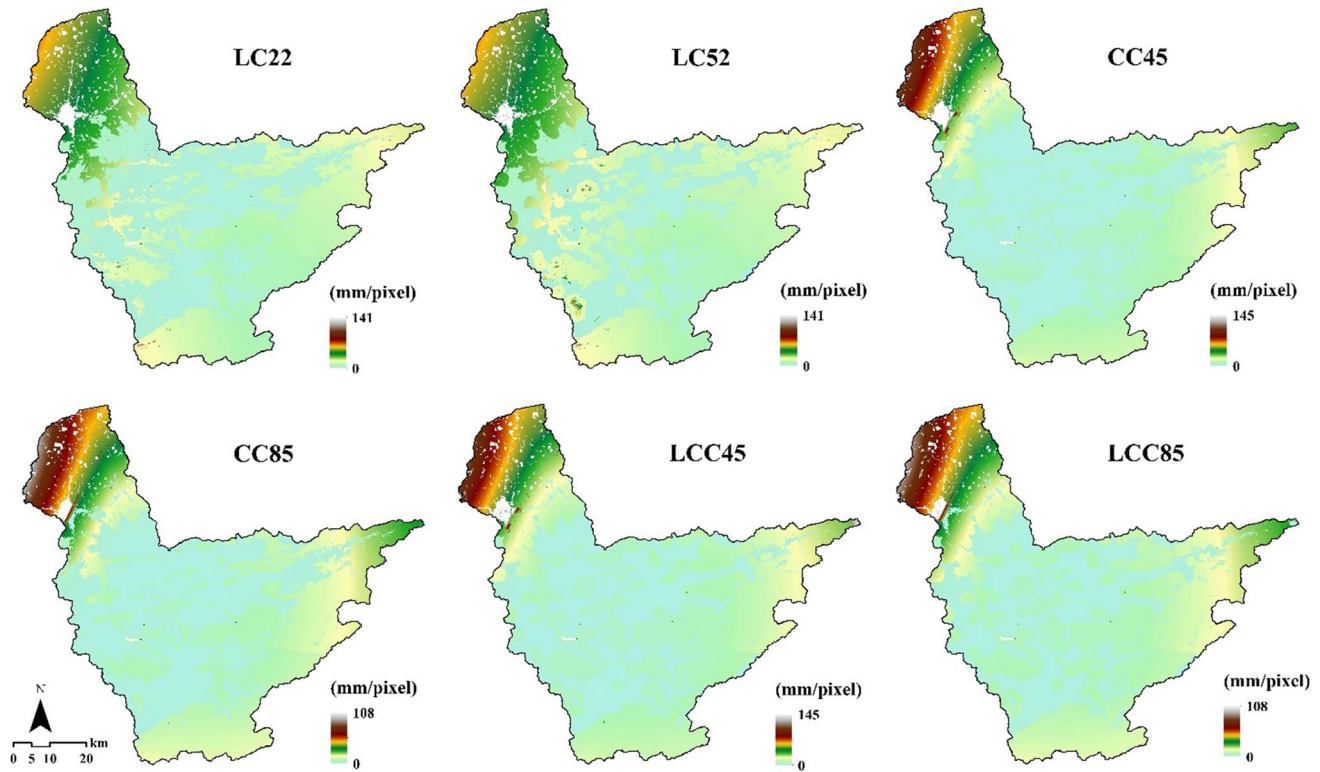
Fig. 5 Maps of water yield resulting from the implementation of all scenarios in InVEST

Table 4 The volume of water yield in the study area predicted in all scenarios and its comparison with the LC22 scenario

Scenario	Water yield		Comparison with LC22	
	Mm^3	m^3 ha^{-1}	Mm^3	%
LC22	23.4	49.5	0	0
LC52	25.1	53.3	1.7	7
CC45	12.3	26.2	− 11.1	− 47
CC85	8.3	17.6	− 15.1	− 65
LCC45	12.9	27.3	− 10.5	− 45
LCC85	8.7	18.4	− 14.7	− 63

(NRMSE) were estimated, resulting in $0.95 < R < 0.99$ and $2\% < NRMSE < 10\%$. These values demonstrate the validity and accuracy of the climate prediction.

Water yield

The InVEST 3.13 software was utilized to model the WY in the study area across six scenarios. The resulting data is demonstrated in Fig. 5 with an average WY of 4.9, 5.3, 2.6, 1.7, 2.7, and 1.8 mm/pixel (30×30 m) for the LC22, LC52, CC45, CC85, LCC45, and LCC85 scenarios, correspondingly. As presented in Table 4, the total volume of WY based on the aforementioned scenarios is estimated as follows: 23.4, 25.1, 12.3, 8.3, 12.9, and 8.7 Mm^3 y^{-1} (on average 49.5, 53.3, 26.2, 17.6, 27.3 and 18.4 m^3 ha^{-1}, respectively). Figure 6 illustrates the classified maps of WY, while Table 5 details the area allocation for each class. The WY of 0–10 mm ha^{-1} is dominant in most of the region, covering 35%, 28%, 49%, 58%, 44% and 55% of its surface in the LC22, LC52, CC45, CC85, LCC45, and LCC85 scenarios, respectively. The WY of more than 50 mm ha^{-1} occupied 20%, 23%, 10%, 8%, 11%, and 8% of the region calculated in the mentioned scenarios, respectively. Figure 7 elucidates the trend of changes in WY at the sub-watershed level in different scenarios. The sub-watersheds 4, 11, 17, 32, 31, and 46 displayed the greatest changes in WY. Table 6 provides the WY for each land use type in all scenarios. Forests had the lowest WY calculated at 8, 18, 3, 2, 3, and 2 m^3 ha^{-1} in the LC22, LC52, CC45, CC85, LCC45, and LCC85 scenarios, respectively, while the highest WY was found in the constructed areas estimated at 654, 642, 162, 82, 163 and 81 m^3 ha^{-1} in the mentioned scenarios, respectively.

Statistical analysis

The G* statistic was utilized to analyze the distribution of WY, as depicted in Fig. 8. The findings indicate that sub-watersheds located in the northern parts of the region were
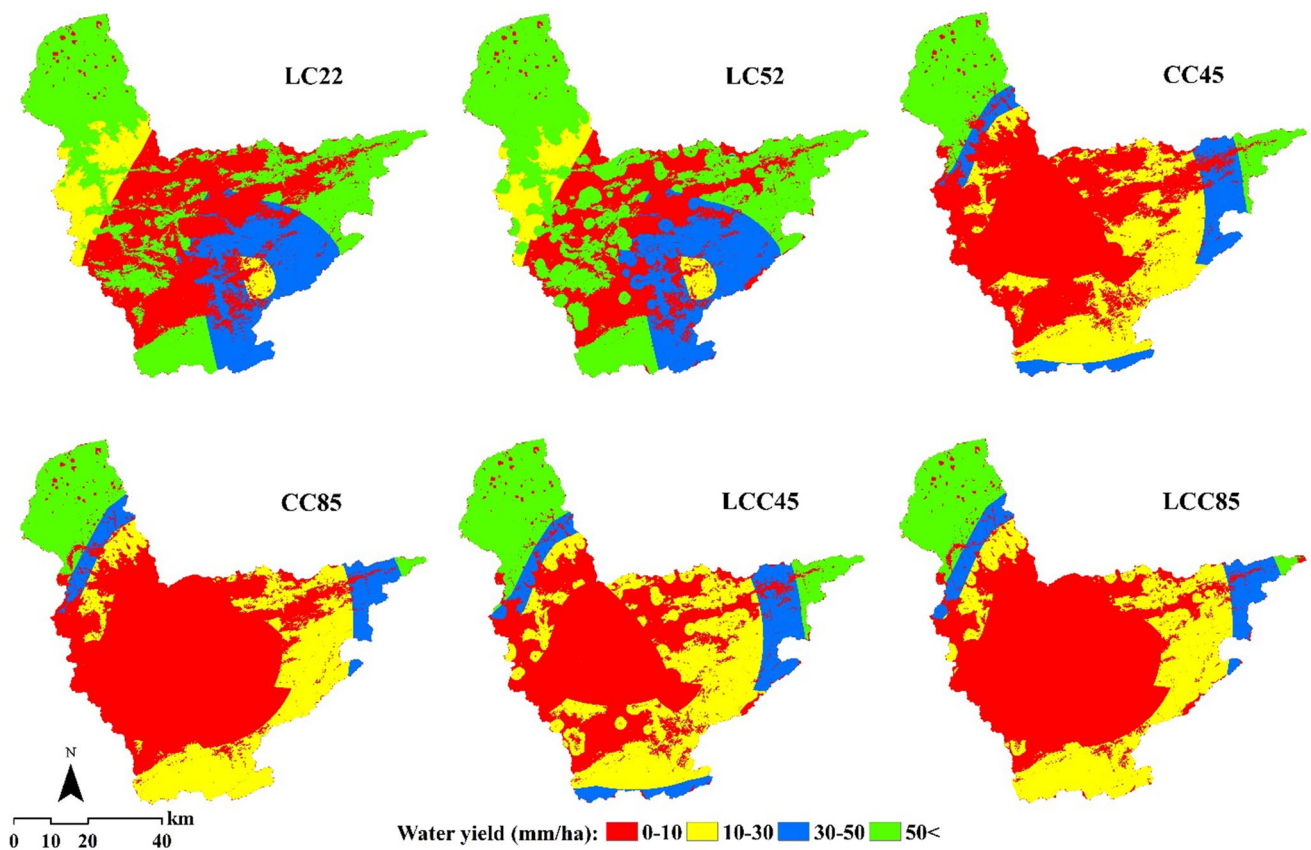
Fig. 6 Classified maps of water yield for all scenarios

Table 5 The area (ha) allocated to each water yield class in all scenarios

Scenario	Water yield classes*			
	I	II	III	IV
LC22	165	116	95	96
LC52	131	115	120	107
CC45	233	162	28	49
CC85	272	143	19	38
LCC45	208	185	29	50
LCC85	260	155	19	38

*I: 0–10, II: 10–30, III: 30–50, and IV: 50 < (mm/ha)

WY hot spots ($0.04 < G* < 0.14$) across different scenarios. Meanwhile, sub-watersheds situated in central parts were cold spots ($0.001 < G* < 0.01$). Additionally, the BLMI statistic was employed to investigate the spatial autocorrelation of WY with elevation, slope, and NDVI, as illustrated in Fig. 9. The estimated Moran's I index for the WY with elevation, slope, and NDVI were -0.53, -0.62, and -0.01, respectively. Furthermore, Fig. 10 clarifies the spatial correlation of WY with elevation, slope, and NDVI analyzed using the GWR in ArcGIS 10.7. The coefficient of
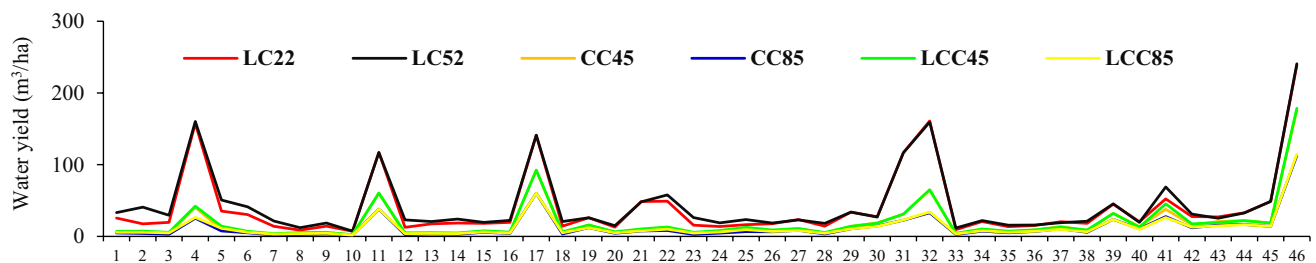

Fig. 7 Water yield changes in the sub-watersheds of the region for each scenario

Table 6 Mean water yield (mm ha^{-1}) for land uses in each scenario

| Scenario	Forest	Rangelands	Agriculture	Built-up area
LC22	8	35	72	654
LC52	18	36	74	642
CC45	3	21	33	162
CC85	2	15	25	82
LCC45	3	21	36	163
LCC85	2	16	26	81

determination (R^2) between WY with elevation, slope, and NDVI was found to be 0.94, 0.90, and 0.96, respectively.

Discussion

From 1992 to 2022, the study area experienced significant land use changes, resulting in land use conversion in 22% of the region. The most notable alterations were the reduction of forests and the increase in agriculture, which covered 17% and 15% of the watershed, respectively. The findings indicated that the Tajan watershed was affected by land use changes during the aforementioned period. These changes reduced natural habitats and altered ecological conditions of the region. Agricultural activities have been one of the most important factors of land use change in the region, which has increased due to population growth and lack of proper land management in the past. Land use change is predicted to be severe from 2022 to 2052, significantly impacting the destruction of the region's forests and reducing habitat quality. Additionally, it can impact water resources and soil conservation in the watershed.

The northern parts of the region had the highest WY, with the central parts having the lowest. This trend was consistent across all scenarios. Higher precipitation and more agriculture and construction in the northern parts were the primary factors behind the WY increase there. This study evaluated WY under various scenarios to measure the impact of climate change and land use, both separately and in combination, on WY variation in the region. The LC22 was the baseline scenario implemented based on land use and climate conditions of 2022. The LC52 scenario illustrated the effect of land use change on water yield, while the CC45 and CC85 scenarios elucidated the impact of climate change. The combined impacts of climate and land use changes on WY were demonstrated by the LCC45 and LCC85 scenarios. The comparison of scenarios indicated that the LC52 scenario yielded the highest water volume (25.1 Mm^3 y^{-1}
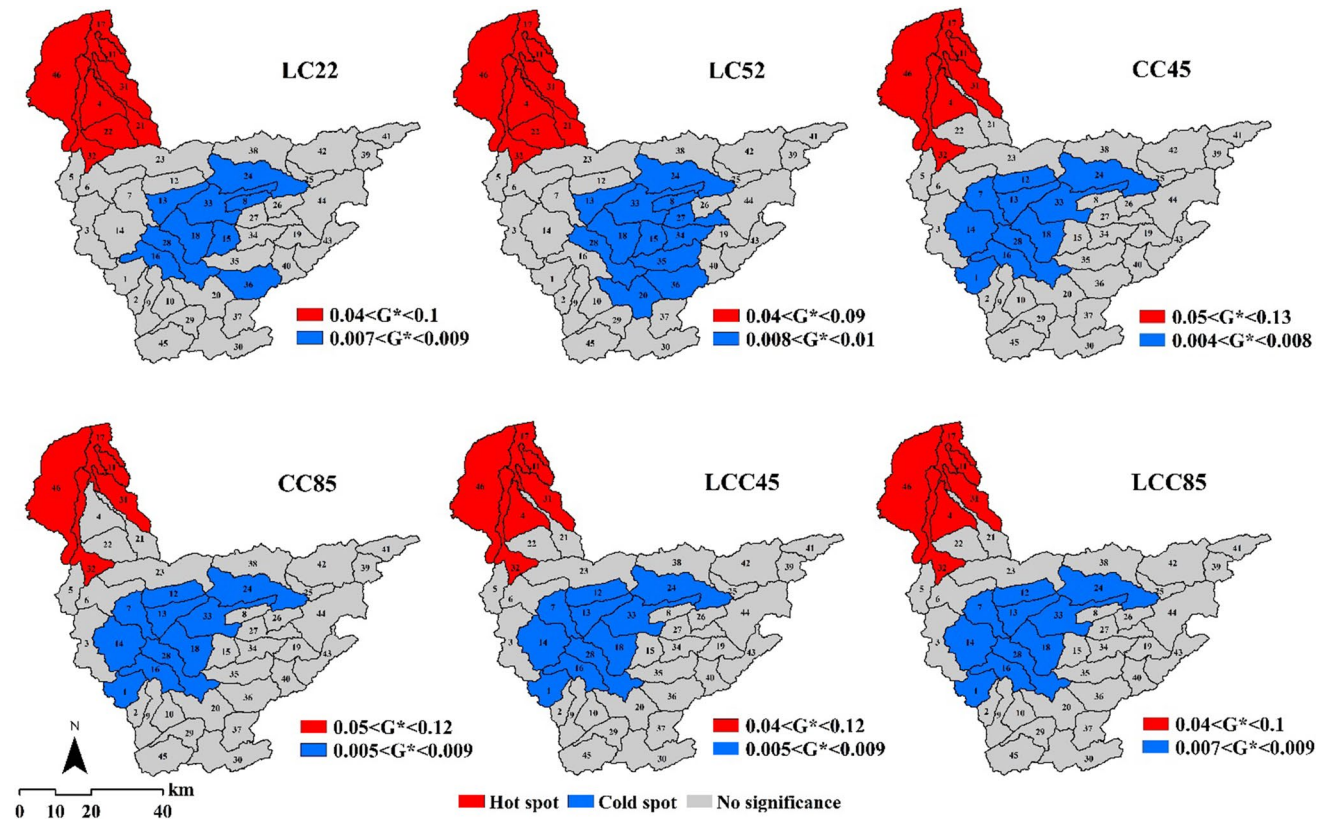
Fig. 8 Results of the Gettis-Ord (G*) statistic to determine hot and cold spots of water yield in all scenarios
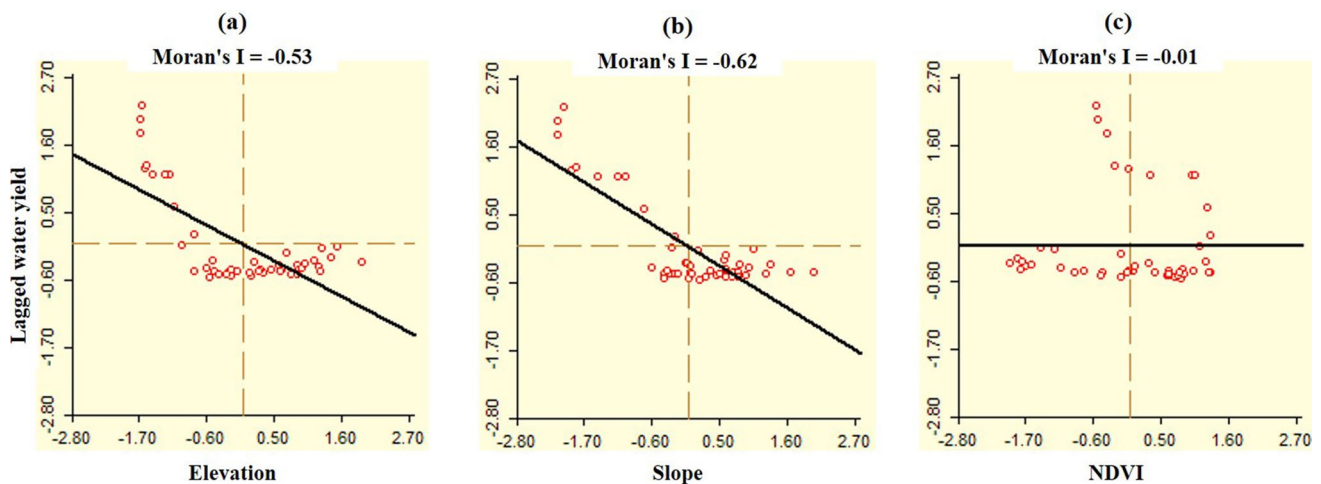
Fig. 9 Results of bivariate local Moran's I (BLMI) to determine the relationship of water yield to **a** elevation, **b** slope, and **c** NDVI
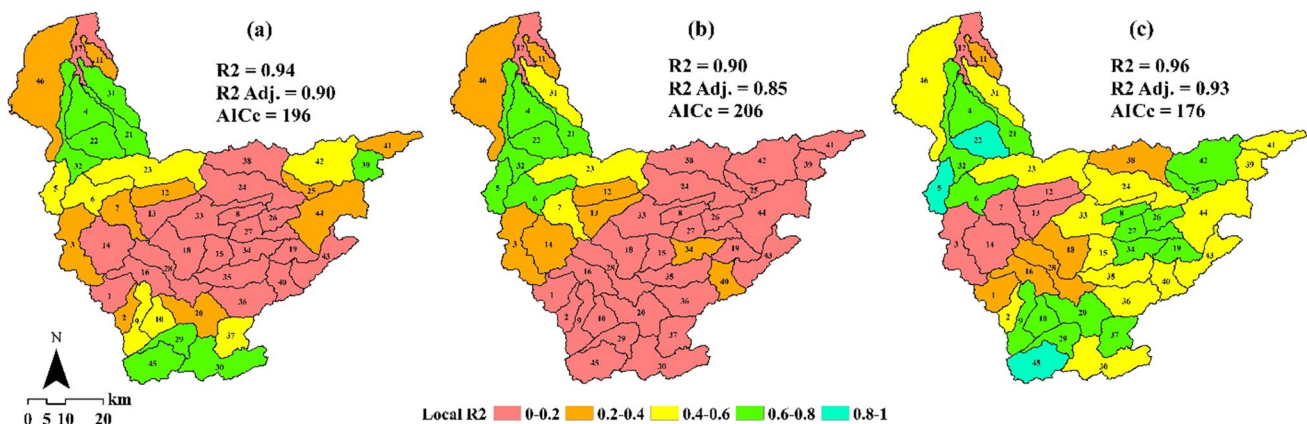

Fig. 10 Spatial correlation of water yield to **a** elevation, **b** slope, and **c** NDVI obtained from geographically weighted regression (GWR)

with an average of 53.3 m^3 ha^{-1}), while the CC85 scenario produced the lowest volume (8.3 Mm^3 y^{-1} with an average of 17.6 m^3 ha^{-1}). Comparison of the LC22 scenario with the LC52, CC45, CC85, LCC45, and LCC85 scenarios exhibited that WY varied by 7%, -47%, -65%, -45%, and -63%, respectively. Additionally, it was demonstrated that land use change contributed 2% to 7% towards an increase in WY, while climate change contributed 47% and 65% (based on RCP45 and RCP85, respectively), towards a reduction in WY. It was also found that climate change based on RCP85 impacts WY variation by 18% compared to RCP45. According to Yifru et al. (2021), WY varied from 8 to 48% in their study area due to the impact of climate change. Pei et al. (2022) confirmed that alterations in WY were predominantly due to climate and land use changes accounting for 88% and 12% respectively. Rafiei-Sardooi et al. (2022) highlighted the significant impact of climate change compared to land

use change on WY. Additionally, Hu and Gao (2020) estimated that climate change had a contribution of over 92% on WY.

The results proved that the WY experienced limited changes under the influence of land use change (based on the LC52 scenario), but severe variations under the effect of climate change (under the CC45 and CC85 scenarios). The impact of climate and land use changes on extreme changes in the WY was also observed under LCC45 and LCC85 scenarios. The study affirmed that the change in climate conditions and land use had a decreasing and increasing effect on WY in the study area, respectively. However, it should be noted that the effects of climate change could be much more severe than those resulted from land use change. Land use change results in variations in vegetation cover and soil permeability, which increases WY. On the other hand, climate change leads to a decrease in precipitation and an increase in evapotranspiration, thus causing a decrease in the total volume of the WY. Yifru et al. (2021) highlighted the

significant impact of climate change scenarios on WY and hydrological processes in comparison to land use change. Pei et al. (2022) demonstrated that climate has a greater impact on WY changes than land use.

The lowest WY of 0–10 mm/ha was mainly observed in central forested areas of the region, while the highest WY (> 50 mm/ha) was estimated in the northern parts that encompassed agriculture and construction activities. The hot spot analysis also revealed that the sub-watersheds located in the northern parts were the primary hot spots of WY, while the central sub-watersheds were designated as cold spots. Built-up areas had the highest WY, while forests had the lowest. The order of WY for land uses was as follows: built-up areas > agriculture > rangelands > forest. The non-permeable built-up surfaces increase WY, while the vegetation in forests helps to preserve and supply water, and thus reduces WY (Guo et al. 2023). Mirghaed and Souri (2023) evaluated the WY of the Shoor River basin in southwest Iran using the InVEST model and found that it is higher in built-up areas than in forest, rangeland, and agriculture. This is in line with the results reported by Yang et al. (2021) and Lang et al. (2017).

Analysis of hotspots in different scenarios revealed that the spatial distribution of WY in sub-watersheds varies due to the impact of climate and land use changes. This fact demonstrates that the effects of climate and land use changes vary depending on the local ecological conditions and human activities that govern each sub-watershed. As a result, the WY also differs among them. These differences can impact the water resources management in each sub-watershed. Hence, Water resource conservation policies and programs should be customized to local conditions in each sub-watershed to mitigate the impact of climate and land use changes.

The spatial autocorrelation analysis revealed that WY has a moderate relationship with elevation and slope (-0.62 < Moran's I < − 0.53). No significant relationship was found with NDVI (Moran's I = − 0.01). These findings indicated that at the sub-watershed level, the spatial distribution of WY is almost opposite to that of slope and elevation in the region. However, there is no relationship between the spatial distribution of WY and vegetation. Mirghaed and Souri (2023) have also reported a significant spatial autocorrelation of WY to elevation and slope. Other studies have also highlighted the significant relationship between topographic features and ecosystem services, particularly with regards to WY (Ma et al. 2021; Shen et al. 2021).

The results of GWR analysis indicated WY has varying local spatial correlations with elevation, slope, and NDVI at the sub-watershed level in the region. Moreover, in most sub-watersheds, WY exhibited a higher local correlation with NDVI compared to elevation and slope. In 37 sub-watersheds, the local spatial correlation of WY with elevation was determined to be low to medium ($0 < R^2 < 0.6$), while in 9 sub-watersheds it was strong ($0.6 < R^2 < 0.8$). Similarly, the local correlation of WY with slope was found to be low to medium in 40 sub-watersheds ($0 < R^2 < 0.4$), and strong in 6 sub-watersheds ($0.6 < R^2 < 0.8$). The local spatial correlation of WY with NDVI was estimated to be low to moderate in 27 sub-watersheds ($0.0 < R^2 < 0.6$), strong in 16 sub-watersheds ($0.6 < R^2 < 0.8$), and very strong ($0.8 < R^2 < 1.0$) in 3 sub-watersheds. These findings suggested that the local spatial correlation of WY with elevation, slope and NDVI is influenced by the geographic location. Despite such differences at the level of sub-watershed, WY had a strong spatial correlation with elevation, slope, and NDVI at the watershed scale ($0.90 < R^2 < 0.96$), implying that topography and vegetation have a significant impact on the WY in the study region. Earlier studies have also referenced the influence of topography and vegetation on the WY (Ahmadi Mirghaed and Souri 2022; Kusi et al. 2020; Mirghaed and Souri 2023; Yang et al. 2021). It was concluded that the impact of topography and vegetation on WY can vary depending on the geographic location. These variations can influence water resource policies, planning, and management in each sub-watershed. Therefore, it is crucial to consider them for effective local water resource management.

Limitations and future prospects

This study has provided a significant understanding of WY under the influence of climate and land use changes in the Tajan watershed, northern Iran. However, it faced certain limitations. The lack of an appropriate database for the study area is considered to be a major limitation in this regard. Some of the inputs of the WY-InVEST model, such as plant rooting depth and Kc coefficient, were prepared based on scientific sources and global databases due to time and cost constraints, which may somewhat affect the results at the local scale. Therefore, it is important to establish a strong database in this regard in Iran for proper assessment and management of water resources.

InVEST evaluates WY based on the difference between annual precipitation and evapotranspiration. However, it has limitations. First, it is not able to evaluate WY at sub-annual scales (seasonal, monthly and daily). Second, it considers the characteristics of rooting depth and Kc coefficient to be the same for a land use type in different areas, which may increase the uncertainty of the results. Third, this model does not consider soil permeability and topographic features, which are important factors affecting WY.

More research is needed to study WY at different scales for water management strategies. Studying the effects of climate and land use changes on WY and their implications for sustainable water resources management is very important. Therefore, the development of advanced simulation methods

to predict and reduce the long-term effects of climate and land use changes on water supply and demand is of particular importance. In future research, it is necessary to consider appropriate approaches to evaluate various environmental, economic, social and political issues related to watersheds in the world, especially in Iran.

Conclusion

This study assessed WY due to climate and land use changes in the Tajan watershed, north of Iran, from 2022 to 2052. The findings indicated that the northern parts of the watershed had the highest WY, while the central parts had the largest WY. In addition, land use changes led to a 2–7% increase in WY, whereas climate change caused a WY reduction of 47% under RCP45 and 65% under RCP85. There was a strong correlation between WY and elevation, slope, and NDVI. Moreover, their correlations can be varied depending on geographical location. In conclusion, this study confirmed that climate change had a greater impact on WY than land-use changes. Additionally, WY can be influenced by local topography and vegetation conditions. This study suggested that managers and planners should adopt appropriate strategies to conserve water in the future regarding water conservation policies, dealing with climate and land use change, and ecological conditions of the region.

Data availability Data will be made on reasonable request.

Declarations

Conflict of interests The authors have not disclosed any competing interests.

References

Abbasian M, Moghim S, Abrishamchi A (2019) Performance of the general circulation models in simulating temperature and precipitation over Iran. Theoret Appl Climatol 135:1465–1483

Ahmadi Mirghaed F, Souri B (2022) Monitoring ecosystem services through land use change in a semiarid region: a case study of the Taluk watershed, southwestern Iran. Int J Environ Sci Technol 19(12):12523–12536

Ambarwulan W, Yulianto F, Widiatmaka W, Rahadiati A, Tarigan SD, Firmansyah I, Hasibuan MAS (2023) Modelling land use/land cover projection using different scenarios in the Cisadane Watershed, Indonesia: implication on deforestation and food security. Egypt J Remote Sens Space Sci 26(2):273–283

Amiri SN, Khoshravesh M, Valashedi RN (2023) Assessing the effect of climate and land use changes on the hydrologic regimes in the upstream of Tajan river basin using SWAT model. Appl Water Sci 13(6):130

Anselin L (1995) Local indicators of spatial association—LISA. Geogr Anal 27(2):93–115

Benra F, De Frutos A, Gaglio M, Álvarez-Garretón C, Felipe-Lucia M, Bonn A (2021) Mapping water ecosystem services: evaluating InVEST model predictions in data scarce regions. Environ Model Softw 138:104982

Brunsdon C, Fotheringham S, Charlton M (1998) Geographically weighted regression. J R Stat Soc: Ser D (stat) 47(3):431–443. https://doi.org/10.1111/1467-9884.00145

Costanza R, d'Arge R, De Groot R, Farber S, Grasso M, Hannon B, Limburg K, Naeem S, O'neill RV, Paruelo J (1997) The value of the world's ecosystem services and natural capital. Nature 387(6630):253–260

Daily GC (1997) Introduction: what are ecosystem services. Nat Ser: Soc Depend Nat Ecosyst 1(1).

Daneshi A, Brouwer R, Najafinejad A, Panahi M, Zarandian A, Maghsood FF (2021) Modelling the impacts of climate and land use change on water security in a semi-arid forested watershed using InVEST. J Hydrol 593:125621

Donohue RJ, Roderick ML, McVicar TR (2012) Roots, storms and soil pores: Incorporating key ecohydrological processes into Budyko's hydrological model. J Hydrol 436:35–50

Droogers P, Allen RG (2002) Estimating reference evapotranspiration under inaccurate data conditions. Irrig Drain Syst 16:33–45

Eastman JR (2012) IDRISI selva manual. Clark University, Worcester

ESRI (2016) ArcGIS help library. https://www.esri.com

Fu B (1981) On the calculation of the evaporation from land surface. Sci Atmos Sinica 5(1):23

Getis A, Ord JK (1992) The analysis of spatial association by use of distance statistics. Geogr Anal 24(3):189–206

Guo Q, Yu C, Xu Z, Yang Y, Wang X (2023) Impacts of climate and land-use changes on water yields: similarities and differences among typical watersheds distributed throughout China. J Hydrol: Reg Stud 45:101294

Hargreaves GH, Samani ZA (1982) Estimating potential evapotranspiration. J Irrig Drain Div 108(3):225–230

Hu Y, Gao M (2020) Evaluations of water yield and soil erosion in the Shaanxi-Gansu Loess Plateau under different land use and climate change scenarios. Environ Dev 34:100488

Huang W, Wang P, He L, Liu B (2023) Improvement of water yield and net primary productivity ecosystem services in the Loess Plateau of China since the "Grain for Green" project. Ecol Ind 154:110707

Kusi KK, Khattabi A, Mhammdi N, Lahssini S (2020) Prospective evaluation of the impact of land use change on ecosystem services in the Ourika watershed. Morocco Land Use Policy 97:104796

Lang Y, Song W, Zhang Y (2017) Responses of the water-yield ecosystem service to climate and land use change in Sancha River Basin, China. Phys Chem Earth Parts a/b/c 101:102–111

Leta MK, Demissie TA, Tränckner J (2021) Modeling and prediction of land use land cover change dynamics based on land change modeler (Lcm) in nashe watershed, upper blue nile basin. Ethiopia Sustain 13(7):3740

Ma S, Qiao YP, Wang LJ, Zhang JC (2021) Terrain gradient variations in ecosystem services of different vegetation types in mountainous regions: vegetation resource conservation and sustainable development. For Ecol Manage 482:118856

Millennium Ecosystem Assessment (2005) Ecosystems and human well-being, vol 5, Island Press, United States of America

Mirghaed FA, Souri B (2023) Contribution of land use, soil properties and topographic features for providing of ecosystem services. Ecol Eng 189:106898

Ord JK, Getis A (1995) Local spatial autocorrelation statistics: distributional issues and an application. Geogr Anal 27(4):286–306

Pei H, Liu M, Shen Y, Xu K, Zhang H, Li Y, Luo J (2022) Quantifying impacts of climate dynamics and land-use changes on water yield service in the agro-pastoral ecotone of northern China. Sci Total Environ 809:151153

Pontius JRG, Suedmeyer B (2004) Components of agreement between categorical maps at multiple resolutions. In: Remote sensing and GIS accuracy assessment, pp 233–251

Rafiei-Sardooi E, Azareh A, Shooshtari SJ, Parteli EJ (2022) Long-term assessment of land-use and climate change on water scarcity in an arid basin in Iran. Ecol Model 467:109934

Semenov MA, Barrow EM, Lars-Wg A (2002) A stochastic weather generator for use in climate impact studies. User Man Herts UK, pp 1–27.

Sharp R, Tallis HT, Ricketts T, Guerry AD, Wood SA, Chapin-Kramer B (2020) InVEST 3.8.0 user's Guide. The Natural Capital Project, Stanford

Shen J, Li S, Liu L, Liang Z, Wang Y, Wang H, Wu S (2021) Uncovering the relationships between ecosystem services and social-ecological drivers at different spatial scales in the Beijing-Tianjin-Hebei region. J Clean Prod 290:125193

Shivakumar BR, Rajashekararadhya SV (2018) An investigation on land cover mapping capability of classical and fuzzy based maximum likelihood classifiers. Int J Eng Technol 7(2):939

Sisay G, Gessesse B, Fürst C, Kassie M, Kebede B (2023) Modeling of land use/land cover dynamics using artificial neural network and cellular automata Markov chain algorithms in Goang watershed, Ethiopia. Heliyon 9(9):e20088

Tijjani SB, Giri S, Woznicki SA (2022) Quantifying the potential impacts of climate change on irrigation demand, crop yields, and green water scarcity in the New Jersey Coastal Plain. Sci Total Environ 838:156538

Viera AJ, Garrett JM (2005) Understanding interobserver agreement: the kappa statistic. Fam Med 37(5):360–363

Wang H, Zhou S, Li X, Liu H, Chi D, Xu K (2016) The influence of climate change and human activities on ecosystem service value. Ecol Eng 87:224–239

Xiao D, Li Liu D, Wang B, Feng P, Bai H, Tang J (2020) Climate change impact on yields and water use of wheat and maize in the North China Plain under future climate change scenarios. Agric Water Manag 238:106238

Yang J, Xie B, Zhang D, Tao W (2021) Climate and land use change impacts on water yield ecosystem service in the Yellow River Basin. China Environ Earth Sci 80(3):1–12

Yifru BA, Chung I-M, Kim M-G, Chang SW (2021) Assessing the effect of land/use land cover and climate change on water yield and groundwater recharge in East African Rift Valley using integrated model. J Hydrol: Reg Stud 37:100926

Zhang L, Hickel K, Dawes W, Chiew FH, Western A, Briggs P (2004) A rational function approach for estimating mean annual evapotranspiration. Water Resour Res. https://doi.org/10.1029/2003WR002710